Fully differential analysis of the electron impact ionization of hydrogen in Debye plasmas

E. Acebal,[1] A. Cuenca,[2] S. Martínez,[1] and S. Otranto[1]
[1)]*Instituto de Física del Sur (IFISUR), Departamento de Física, Universidad Nacional del Sur (UNS), CONICET, Av. L. N. Alem 1253, B8000CPB - Bahía Blanca, Argentina.*
[2)]*Departamento de Física, Universidad Nacional del Sur (UNS), Av. L. N. Alem 1253, B8000CPB - Bahía Blanca, Argentina.*

(*Electronic mail: emiliano.acebal@uns.edu.ar)

(Dated: 19 October 2021)

In this work, electron impact ionizing collisions on atomic hydrogen embedded in weakly coupled plasmas are studied at impact energies of 80 eV and 150 eV. Fully differential cross sections calculated by means of a distorted wave model which explicitly considers the screening effect among the three interacting particles in the final state are presented and analyzed. Compared to the unscreened case, clear differences in shape and magnitude are found for the dominant structures, the binary and recoil peaks, suggesting that the role played in the collision by the different particles varies with the Debye screening length. A scaling law for the fully differential cross section in terms of the nuclear charge Z, first proposed by Kornberg and Miraglia in the photo-double ionization context, is shown to also hold for the electron impact ionization of hydrogenic ions in the present screened context.

I. INTRODUCTION

The study of charged particle collisions with atoms and molecules represents one of the most interesting and long-lasting problems in atomic physics research. Besides its inherent importance in a basic science perspective, there is also the potential role these processes play in many areas, like fusion plasmas, astrophysics and radiotherapy among others. A particular example is provided by charge exchange spectroscopy. This diagnostic tool allows to infer the plasma temperature, its rotation and the amount of impurities inside a tokamak reactor from the photonic emission that follows charge exchange reactions with H(1s) and H^*(n=2)[1,2]. In astrophysics, x-ray emission from comets has been found to originate in the electronic deexcitation that follows charge exchange processes between the solar wind ions and the cometary gases in the coma. In this sense, charge exchange cross sections have been used to reproduce the spectral analysis of the Chandra x-Ray-Observatory survey[3–5]. In radiotherapy, electron emission cross sections of different level of differentiability are used as input data for transport simulation codes during the planning stage of cancer irradiation treatments[6–10]. While many of these contexts involve complex molecules like H_2O, CO_2, CH_4, DNA-bases etc., it is worth noting that hydrogen or hydrogenic ions have been largely used in quantum mechanical and classical analyses as primary substitutes of those targets or the resulting ions. This obeys, on the one hand, to the fact that the ionization potential of hydrogen is similar to those obtained for their least bound orbital. On the other hand, bound and continuum states for the two-body Coulomb problem can be expressed in analytical closed form, easing calculations that can otherwise turn prohibitive.

The dynamics of electron emission processes can be studied in terms of the Fully Differential Cross Sections (FDCS). These provide a complete picture of the collision events, since the momenta of all the fragments involved are resolved. The first FDCS for the single ionization process of helium by electron impact were measured in the late 1960s[11,12]. During the next five decades, FDCS for electron impact ionization of different atomic and molecular targets like H, He, Ar, H_2O, among others, have been reported from several groups working worldwide[13–23]. Moreover, recently the Heidelberg group succeeded in measuring FDCS for the electron impact ionization of H_2 molecular targets, determining their specific orientation at the instant that each collision event took place[24]. This clearly shows the actual capabilities of reaction microscopes and a promising perspective regarding the study of collisions with complex molecules. From a theoretical point of view, we can distinguish the applied methods in two families: perturbative treatments and numerically intensive. The former are mainly represented by distorted wave methods, like the distorted wave Born approximation (DWBA)[23,25], the three distorted wave Born approximation (3DWBA) (among which we include the three Coulomb Born approximation (3CBA) and many of the proposed variations in terms of coordinate and momentum dependent charges)[26–29], and the continuum distorted wave-eikonal initial state (CDW-EIS) model[30–34] of wide use in the ion-atom and ion-molecule context[7,35], and in principle can be extended to deal with complex molecular targets at a considerably inferior computational cost. The latter rely on very powerful computational capabilities, and have proved to accurately describe the reported experimental data for light atomic targets like H and He, and have been recently extended to Kr and Si[36–41]. Nevertheless, complex molecular targets still represent a challenge for these methods, even in a one-active electron approximation[42].

The above cited studies entirely correspond to collisions involving gas phase targets in such low densities that the target atom/molecule can be considered to be isolated from its surroundings. In contrast, laboratory and astrophysical plasma environments represent a completely different scenario. The interactions among specific particles in these contexts are now screened, in a lesser or greater extent, according to the temperature and density of the medium. As a result, not only the electronic structure of atoms and molecules is affected compared to the unscreened case, but also the outcomes of dif-

ferent collisional processes like photon excitation and ionization, electron/positron impact excitation and ionization, and charge exchange, excitation and ionization during ion impact. In particular, weakly coupled plasmas, for which interparticle interactions can be described by means of the Debye-Hückel potential, have prompted a large set of theoretical studies during the past few decades (see Ref. [43] for a recent review). For electron impact collisions, convergent-close-coupling calculations established for H and He targets that as the strength of the screening of the medium increases, the total ionization cross section increases while the excitation cross section diminishes[44,45]. Other recent studies focused on singly differential ionization cross sections in energy (SDCS) for fast electron impact ionization of hydrogen ions in their 2s or 2p states. These studies were restricted to the low energy part of the spectrum of ejected electrons and analyzed how the strength of the screening affects the shape and positions of resonances[46]. Finally, and up to our knowledge, the only published study of the electron impact ionization of hydrogen in Debye plasmas at the fully differential level is that of Li *et al.*[47]. In that work, the authors used the numerically intensive Exterior Complex Scaling method to analyze the punctual case of coplanar equal-energy-sharing at an electron impact energy of 15.6 eV. This corresponds for the unscreened case to the region in which the Wannier threshold law is considered to be valid[48].

In this work we study the electron impact ionization of screened hydrogenic ions in their ground state at the fully differential level at impact energies of 80 eV and 150 eV. These energies are representative of the region at which the total ionization cross section peaks for the unscreened case, and are large enough to allow the implementation of perturbative models. The theoretical method employed is the 3DWBA which is hereby extended to a Debye plasma environment. In contrast to the work of Li *et al.*, angular distributions for the slow electron resulting from asymmetric collisions will be analyzed at different fixed angles for the fast electron. Main focus will be placed in describing the sensitivity of the structures of the FDCS on the screening strength for different projectile scattering angles, and tracing the physical origin of the changes they exhibit.

In the next section, we describe the theoretical method, while in Sec. III, we present and analyze our results. Conclusions are drawn in Sec. IV. Atomic units are used throughout this work unless otherwise stated.

II. THEORY

The FDCS for the single ionization process is given by[49]

$$\frac{d^5\sigma}{dE_2 d\Omega_1 d\Omega_2} = (2\pi)^4 \frac{k_1 k_2}{k_0}\left[\frac{1}{4}\left|T_{fi}^D + T_{fi}^E\right|^2 + \frac{3}{4}\left|T_{fi}^D - T_{fi}^E\right|^2\right]. \tag{1}$$

Here, k_0, k_1 and k_2 represent the impinging projectile, the scattered projectile and the emitted electron momenta, respectively. T_{fi}^D and T_{fi}^E are the direct and exchange transition amplitudes, with $T_{fi}^E(\boldsymbol{k}_1,\boldsymbol{k}_2) = T_{fi}^D(\boldsymbol{k}_2,\boldsymbol{k}_1)$.

In what follows we describe the 3DWBA that is used throughout this work. The interaction between two particles with charges Z_i and Z_j separated at a distance r_{ij} in our plasma environment is described by the Debye-Hückel model potential:

$$V(r_{ij}) = \frac{Z_i Z_j}{r_{ij}} e^{-\frac{r_{ij}}{r_D}}. \tag{2}$$

In this expression, the parameter r_D is the denominated Debye screening length and will be used hereafter as the indicator of the level of screening in the environment. Nevertheless, it is worth noting that in plasma studies the use of its inverse $\lambda = {r_D}^{-1}$ is quite common. This parameter is related to the plasma frequency ω_P and its thermal velocity v_T through $\lambda = \omega_P/v_T = \sqrt{4\pi e^2 n_e/(k_B T_e)}$, where k_B is the Boltzmann constant, e is the electron charge, and n_e and T_e are the plasma-electron density and temperature, respectively.

Then, for a Born initial state the transition amplitude for the ionization process can be written as

$$T_{fi} = \langle \Psi_f^- | V_I | \psi_i \rangle, \tag{3}$$

where the initial wave function ψ_i is given by the screened hydrogen ground state wave function ϕ_i times an incident plane wave for the incoming projectile:

$$\psi_i = \frac{1}{(2\pi)^{3/2}} e^{i\boldsymbol{k}_0\cdot\boldsymbol{r}_1}\phi_i(\boldsymbol{r}_2). \tag{4}$$

Here $\boldsymbol{r}_1$ and $\boldsymbol{r}_2$ are the projectile electron and target electron coordinates with respect to the nucleus. We have employed Salvat's code[50] to obtain the ground state wave functions ϕ_i for the different r_D-values considered. This code numerically solves the Schrödinger equation for a particle of mass M in the field of a central potential.

The interaction potential V_I is given by the non-resolved part of the hamiltonian by the initial state ψ_i:

$$V_I(\boldsymbol{r}_1,\boldsymbol{r}_2) = -\frac{Z}{r_1} e^{-\frac{r_1}{r_D}} + \frac{1}{r_{12}} e^{-\frac{r_{12}}{r_D}}, \tag{5}$$

where $\boldsymbol{r}_{12} = \boldsymbol{r}_1 - \boldsymbol{r}_2$ and Z is the charge of the nucleus.

Finally, the final-state wave function Ψ_f^- is written as

$$\Psi_f^- = \chi^-(\boldsymbol{k}_1,\boldsymbol{r}_1)\,\chi^-(\boldsymbol{k}_2,\boldsymbol{r}_2)\,\zeta^-(\boldsymbol{k}_{12},\boldsymbol{r}_{12}), \tag{6}$$

with $\boldsymbol{k}_{12} = (\boldsymbol{k}_1 - \boldsymbol{k}_2)/2$. The wave function $\chi^-(\boldsymbol{k}_i;\boldsymbol{r}_i)$ with $i = 1,2$ represents the final-state continuum wave function for an electron in the field of the nucleus and is given by the following partial wave expansion:

$$\chi^-(\boldsymbol{k}_i;\boldsymbol{r}_i) = \sum_{l=0}^{\infty} \frac{(2l+1)}{k_i r_i} i^l e^{-i\delta_l} u_l(k_i,r_i) P_l(\hat{\boldsymbol{k}}_i\cdot\hat{\boldsymbol{r}}_i). \tag{7}$$

Here, $P_l(\hat{\boldsymbol{k}}_i \cdot \hat{\boldsymbol{r}}_i)$ are the Legendre polynomials and δ_l is the phase shift with respect to the plane wave. The radial wave function $u_l(k_i, r_i)$ fulfills the equation,

$$\left[-\frac{1}{2}\frac{d^2}{dr_i^2} + \frac{l(l+1)}{2r_i^2} + V(r_i)\mu_i\right] u_l(k_i, r_i) = \frac{k_i^2}{2} u_l(k_i, r_i) \quad (8)$$

and, together with δ_l, can be obtained through Salvat's code[50]. In this expression, μ_i is the reduced mass (either for the projectile-nucleus or the emitted electron-nucleus subsystems) and can be safely approximated to 1. The potential $V(r_i)$, represents the interaction of an electron (either the emitted electron or the projectile) with the target nucleus and its functional form is given by Eq. (2).

On the other hand, the wave function $\zeta^-(\boldsymbol{k}_{12}, \boldsymbol{r}_{12})$ represents the screened projectile-electron interaction and is given by

$$\zeta^- = \chi^-(\boldsymbol{k}_{12}, \boldsymbol{r}_{12})(2\pi)^{3/2} e^{-i\boldsymbol{k}_{12}\cdot\boldsymbol{r}_{12}}. \quad (9)$$

Since the mass of the particles in this case is the same ($m_1 = m_2 = 1$), the reduced mass in Eq. (8) is $\mu_{12} = m_1 m_2/(m_1 + m_2) = 1/2$. Therefore, to obtain $\chi^-(\boldsymbol{k}_{12}, \boldsymbol{r}_{12})$ the interaction potential of Eq. (2) has been multiplied by $1/2$ in Salvat's code. By doing so, we have verified that our final wave function reduces to the well known 3C function[26,51] when the screening is removed.

To evaluate the transition amplitude T_{fi}, we have performed a six-dimensional integration by the adaptive Vegas Monte Carlo algorithm[52]. The wavepacket approach of Malcherek and Briggs was used to treat the continuum-continuum transition for the projectile[53]. In contrast to non-screened environments, in which the electron-electron interaction in the final state is usually described by means of a Kummer function, or in a much simpler form, a Gamow factor[23,25–27,30–34], the present context requires the computation of a large set of partial waves for each emission angle. As a result, the computational effort needed to compute the angular distributions increases.

III. RESULTS

In this section we present the ionization FDCS for r_D values between 1 and 100 a.u.. The former value corresponds to the most screened case we analyzed and the latter to the least one, letting aside calculations for the unscreened case. This range pertains to inertial confinement fusion plasmas ($T_e \sim 6\times10^6 - 10^8 K$, $n_e \sim 10^{22} - 10^{26} cm^{-3}$) and laser produced plasmas ($T_e \sim 5\times10^5 - 3\times10^6 K$, $n_e \sim 10^{19} - 10^{21} cm^{-3}$)[54]. We consider electron impact energies of 80 eV and 150 eV. As already stated, these energies are representative of the region at which the total ionization cross section peaks, or in other words, the ionization probability maximizes. The analysis of the role played by the different physical mechanisms at these impact energies is, therefore, expected to improve our overall comprehension of the collision process. The emission

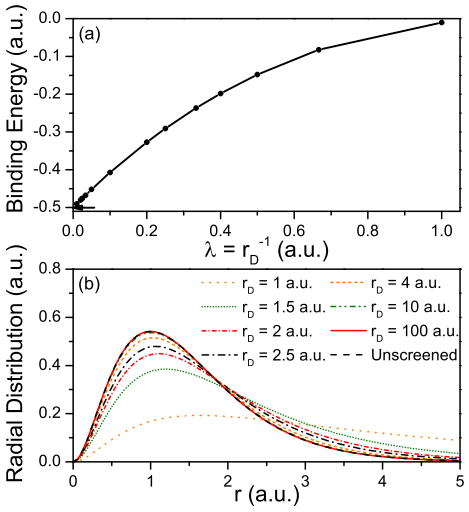

FIG. 1. (a) Binding energy as a function of the inverse of the Debye screening length and (b) radial distributions of the hydrogenic ground states with charge $Z = 1$ for different r_D values.

geometries studied involve projectile scattering angles of $-4°$, $-10°$ and $-15°$ and secondary electron emission energies of 5 eV and 10 eV. These have been previously considered in former experimental and theoretical analyses for the unscreened case[55,56]. For a given electron emission energy, the momentum transferred by the projectile during the collision increases with the scattering angle. Therefore, most of the overall ionization yield is expected to be provided by low scattering angles like those considered in this work. Present studies only consider the electronic emission in the scattering plane defined by the momentum vectors $\boldsymbol{k}_0$ and $\boldsymbol{k}_1$.

In the first place, in Fig. 1(a) we present the ground state energies of the hydrogen atom ($Z = 1$) as a function of the inverse of the Debye screening length r_D. As the screening length increases (decreasing screening), the binding energy tends to the unscreened ground state energy of atomic hydrogen -0.5 a.u., which corresponds to the asymptotic limit of the Debye-Hückel model potential defined in Eq. (2) when r_D tends to infinity. In contrast, as the screening length decreases (increasing screening), the binding energy rapidly increases reaching an almost null value for $r_D = 1$ a.u.. This particular value is very close to the denominated critical screening length of 0.83991 a.u., which represents the minimum r_D-value needed for a bound state to exist in a Debye plasma environment[57]. In Fig. 1(b) we analyze the radial distributions of the ground state wave function of hydrogen as a function of r_D. It can be observed that the screening effect turns visually noticeable only for r_D values lower than 10 a.u. ($\lambda > 0.1$ a.u.), a value at which the binding energy has already increased by

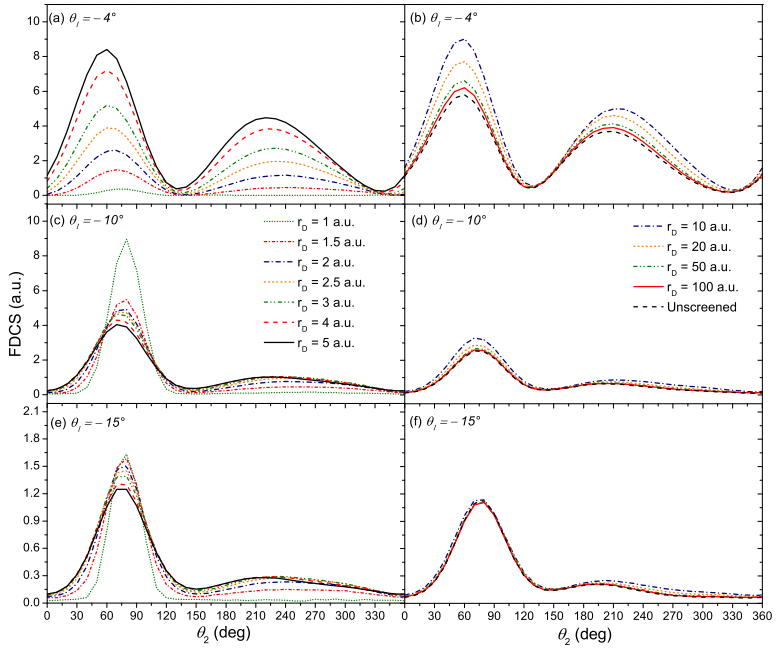

FIG. 2. Fully differential cross sections for electron impact ionization of hydrogenic targets of charge $Z = 1$ embedded in Debye-Hückel plasmas with different screening lengths as a function of the secondary electron emission angle. Left column: $r_D = 1 - 5$ a.u.. Right column: $r_D = 10 - 100$ a.u.. The unscreened asymptotic limit is also presented. The impact energy is $E_0 = 150$ eV and the secondary electron emission energy is $E_2 = 5$ eV. The projectile scattering angles are (a) and (b) $-4°$, (c) and (d) $-10°$, and (e) and (f) $-15°$.

about 20 % (Fig. 1(a)). As r_D decreases below 10 a.u. the radial distribution extends to larger r-values, exhibiting a strong variation for $r_D < 2$ a.u.. Thus, the overall physical picture of the target system embedded in a Debye-Hückel plasma, as the screening effect increases, is one in which the radial distribution of the electron extends to greater distances from the nucleus with lower ionization potentials.

In Fig. 2 we analyze the FDCS corresponding to an impact energy of 150 eV. The secondary electron is emitted with an energy of 5 eV for the three projectile scattering angles considered. Results are shown for Debye screening lengths of 1, 1.5, 2, 2.5, 3, 4, and 5 a.u. in the left column, and 10, 20, 50 and 100 a.u. in the right column. For the unscreened case we present calculations made with the 3CBA. In Figs. 2(a) and 2(b) the projectile is scattered with an angle $\theta_1 = -4°$ with respect to the incoming beam direction. As a general trend, we observe the well known two-peak structure, conformed by the binary peak, near the momentum transfer direction, and the recoil peak along the opposite direction.

Starting from $r_D = 1$ a.u., the magnitude of the cross section increases and reaches its top value for $r_D = 10$ a.u.. For

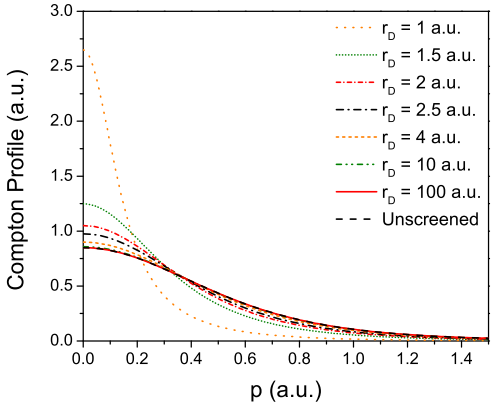

FIG. 3. Compton Profiles of the hydrogenic ground states with charge $Z = 1$ for different r_D values.

$r_D > 10$ a.u., the cross section slowly decreases towards the unscreened case results. Regarding the positions at which the mentioned structures peak, a clear and sustained shift of the recoil peak towards $\theta_2 = 210^\circ$ can be observed, suggesting an increasing role of the postcollisional interaction as the screening is decreased. In contrast, the binary peak seems less sensitive to the screening level and exhibits a small shift towards lower θ_2-values as r_D increases. The shift in this case is attributable to the variation in direction of the momentum transfer vector $\boldsymbol{q} = \boldsymbol{k}_0 - \boldsymbol{k}_1$ as the Debye screening length increases.

Increasing the projectile scattering angle to $\theta_1 = -10^\circ$ in Figs. 2(c) and 2(d), we observe a similar behavior in the recoil region as a function of the Debye screening length r_D, with the magnitude of the recoil peak not showing significant variations. In contrast, in the binary peak region we observe a very focused and pronounced structure for the smallest r_D value considered. As r_D increases, the binary peak gets wider and smaller in magnitude until it reaches the asymptotic unscreened limit. In Figs. 2(e) and 2(f), when the scattering angle is increased to $\theta_1 = -15^\circ$ a similar behavior is observed in the entire emission region, although the binary peak magnitude does not decrease as much as in the previous case when the Debye screening length increases.

As a general trend, for the three different scattering angles analyzed in Fig. 2 the binary peak gets wider as the Debye screening length is increased. It is well known that the width of the binary peak is linked to the Compton profile of the target initial state[58]. Therefore, in Fig. 3 we show the target Compton profile calculated with the hydrogen ground state obtained for different r_D values. We observe that for r_D = 1 a.u., the Compton profile is narrow and with a large magnitude. As the Debye screening length increases, this distribution decreases its magnitude and gets wider. In this sense, we can attribute the widening of the FDCS in Fig. 2 as r_D is increased, to the widening of the Compton profile of the target initial state observed in Fig. 3.

The main difference observed when the scattering angle is increased from -4° in Figs. 2(a) and 2(b) to -10° (Figs. 2(c) and 2(d)) is that the binary peak of the FDCS for the most screened case (r_D = 1 a.u.) considerably increases its magnitude. The binary peak can be viewed, in a classical representation, as resulting from a binary collision between the projectile and the bound electron. To shed light on this behavior, in Fig. 4 we analyze the magnitude of the binary peak as a function of the Debye screening length for the three scattering angles considered. For $\theta_1 = -4^\circ$, the probability to emit an electron in a binary encounter is minimum for r_D = 1 a.u.. Increasing the Debye screening length, we observe that this probability increases until it reaches a maximum for r_D = 10 a.u., after which it begins to decrease towards the asymptotic unscreened limit, as we observe in Fig. 2(b). On the other hand, for $\theta_1 = -10^\circ$ this probability is strictly descendent, with the maximum value attained for r_D = 1 a.u. The same occurs for $\theta_1 = -15^\circ$, but with this probability remaining almost constant.

We can explain these differences for r_D = 1 a.u., by analyzing the momentum vectors of this process. The secondary

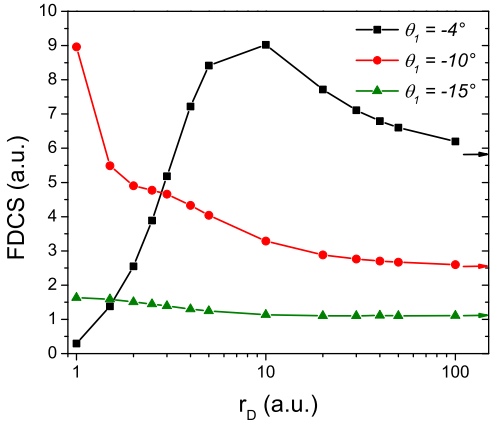

FIG. 4. Fully differential cross section binary peak magnitude as a function of the Debye screening length for three different scattering angles. The impact energy is $E_0 = 150$ eV and the secondary electron emission energy is $E_2 = 5$ eV. The horizontal arrows indicate the unscreened asymptotic limits.

electron can only be emitted with momentum $\boldsymbol{k}_2$ in a binary encounter with the projectile, if the momentum transfer from the projectile to the target is sufficient for this process to take place ($|\boldsymbol{q}| > |\boldsymbol{k}_2|$). If $|\boldsymbol{q}| < |\boldsymbol{k}_2|$, the emission can be reached only via momentum exchange with the nucleus. Hence, when the electron and the recoil ion interaction is minimized, as it occurs for the most screened case r_D = 1 a.u., then the secondary electron finds no possible source to acquire the amount of momentum needed to be emitted with the energy under consideration. In the three cases analyzed in Fig. 2 the secondary electron leaves the collision region with momentum magnitude $|\boldsymbol{k}_2|$ = 0.606 a.u., while the momentum transfer magnitude $|\boldsymbol{q}|$ for a Debye screening length of r_D = 1 a.u. is 0.237 a.u., 0.576 a.u. and 0.861 a.u. for $\theta_1 = -4^\circ, -10^\circ$, and -15°, respectively. In this sense, we can see that for the smallest scattering angle considered the momentum transfer is smaller than the emitted electron momentum and electronic emission can only be attained thanks to the Compton profile of the target electron. Therefore, the probability that ionization occurs for $\theta_1 = -4^\circ$ becomes low compared to the $\theta_1 = -10^\circ$ case, in which the momentum transfer magnitude is close enough to the emitted electron momentum, and the ionization of the target can take place with almost no participation of the nucleus. For $\theta_1 = -15^\circ$ the projectile momentum transfer is larger than $\boldsymbol{k}_2$ and the nucleus needs again to take part in the momentum exchange for the process to take place.

As the Debye screening length is increased, the interaction between the secondary electron and the recoil ion gains relevance and changes in the binary-recoil ratios are expected, leading to variations in the magnitude of the binary peak. For $\theta_1 = -4^\circ$, the extended spatial range of the electron-

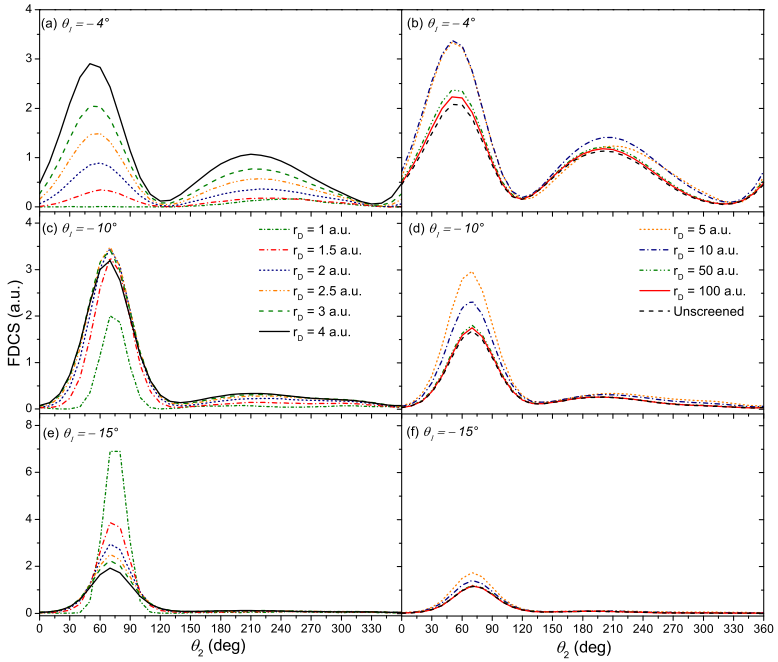

FIG. 5. Same as Fig. 2, but for $E_2 = 10$ eV. Left column: $r_D = 1 - 4$ a.u.. Right column: $r_D = 5 - 100$ a.u.. The unscreened asymptotic limit is also presented.

nucleus interaction increases the probability of momentum exchange among particles. As a result, the binary peak increases, exhibits a maximum and then decreases towards the unscreened limit. The latter suggests that as the screening length increases, different emission geometries are favoured. For $\theta_1 = -10°$, in which the classical binary encounter condition is almost fulfilled, and the classical picture of a binary encounter followed by a secondary collision of the already emitted electron with the nucleus gains relevance, the maximum value is attained for r_D = 1 a.u. The fact that the binary peak magnitude decreases with increasing r_D can be also understood in terms of the increasing role of the secondary collisions between the emitted electron and the target nucleus, and can inferred from the appearance of a recoil peak. The same situation applies to $\theta_1 = -15°$, although now the recoil ion plays a role at all times.

In Fig. 5 we increase the emitted electron energy to 10 eV. In this case, the emitted electron momentum is 0.857 a.u. and the projectile momentum transfers for r_D = 1 a.u. are 0.255 a.u., 0.580 a.u., and 0.859 a.u., for $\theta_1 = -4°, -10°$, and $-15°$, respectively. While in general terms the FDCS follow the same trends already described for the 5 eV case, it is worth highlighting some points regarding these new geometries. For

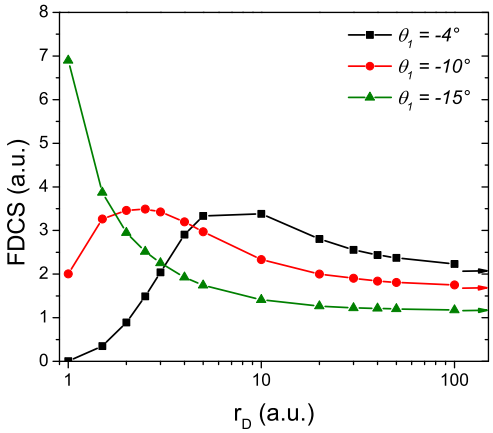

FIG. 6. Same as Fig. 4, but for $E_2 = 10$ eV.

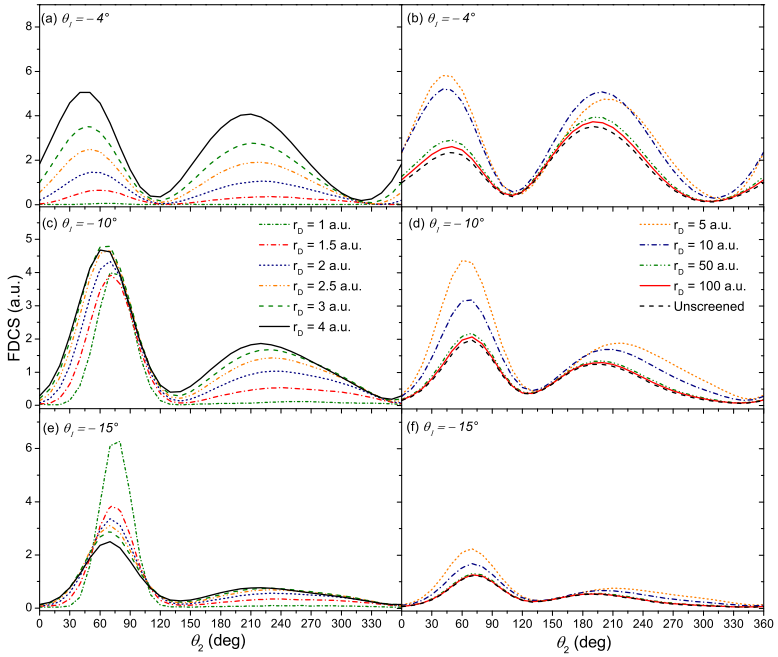

FIG. 7. Same as Fig. 5, but for $E_0 = 80$ eV and $E_2 = 5$ eV.

$\theta_1 = -4°$ (Figs. 5(a) and 5(b)) a recoil peak is obtained for r_D = 1 a.u. but no binary peak is present. Again, this particular geometry requires the momentum exchange between the emitted electron and the target nucleus to take place. Compared to the 5 eV case, the amount of momentum the nucleus needs to provide to the electron to be emitted with 10 eV is now larger, and cannot be solely attained from the Compton profile of the target electron. The small recoil peak is consequence of the small spatial window in which a secondary collision can take place. For $\theta_1 = -10°$ (Figs. 5(c) and 5(d)) the binary peak for r_D = 1 a.u. is no longer as large as for the 5 eV case with respect to the other Debye screening lengths. In this case, the magnitude of this peak increases until r_D = 3 a.u., after which it decreases towards the asymptotic unscreened limit. The classical binary encounter, now happens to occur for $\theta_1 = -15°$ when the emitted electron energy is 10 eV, and no recoil structure is observed. The binary peak for r_D = 1 a.u. is the highest and narrowest one, and then it decreases its magnitude towards the asymptotic unscreened limit. These statements can be corroborated and further analyzed by inspecting the magnitude of the binary peak against the Debye screening length for the three different scattering angles, what is shown in Fig. 6.

In order to analyze if all these features are consistent at

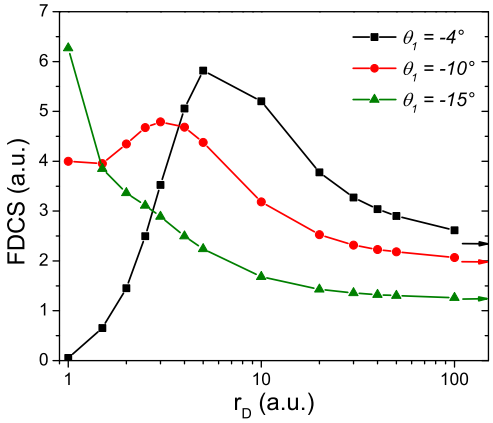

FIG. 8. Same as Fig. 4, but for $E_0 = 80$ eV and $E_2 = 5$ eV.

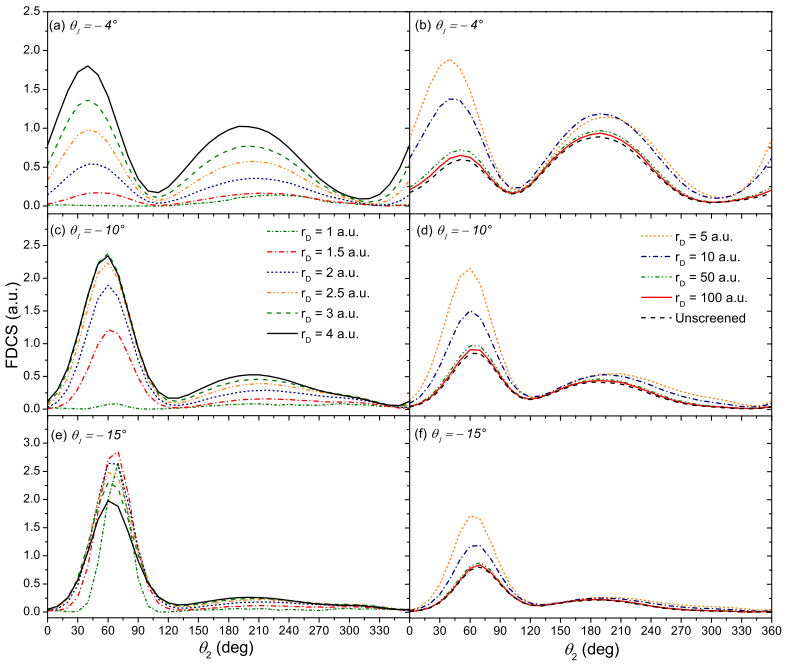

FIG. 9. Same as Fig. 5, but for $E_0 = 80$ eV and $E_2 = 10$ eV.

lower impact energies, we calculate FDCS at an electron impact energy of 80 eV. In Figs. 7 and 8 we consider an emitted electron energy of 5 eV. In this case, the emitted electron momentum magnitude is 0.606 a.u. and the momentum transfer magnitudes for $r_D = 1$ a.u. are 0.185 a.u., 0.423 a.u., and 0.628 a.u., for $\theta_1 = -4°, -10°$, and $-15°$, respectively. The ratio of the momentum transfer magnitudes with respect to the electron momentum are almost the same as in the previous case, when the impact energy was 150 eV and the secondary electron was emitted with 10 eV. Hence, we expect similarities to appear between these two cases. Nevertheless, we observe in Fig. 7(b) that at $r_D = 10$ a.u. the binary-recoil peak ratio inverts, and the recoil peak remains larger than the binary peak until the asymptotic unscreened limit. It is worth mentioning that a larger recoil peak was observed for 54.4 eV electron impact ionization of unscreened hydrogen[31,56] and therefore this feature was not unexpected at the impact energy explored.

In Figs. 9 and 10 we complement our analysis at the impact energy of 80 eV, by increasing the emission energy to 10 eV. We note in this case that the inversion of the binary-recoil peak ratio for $\theta_1 = -4°$ takes place at a larger r_D value compared to the 5 eV case. Moreover, the maximum of the binary peak is not attained for $r_D = 1$ a.u. for any of the three scattering angles considered. This can be again explained by taking into

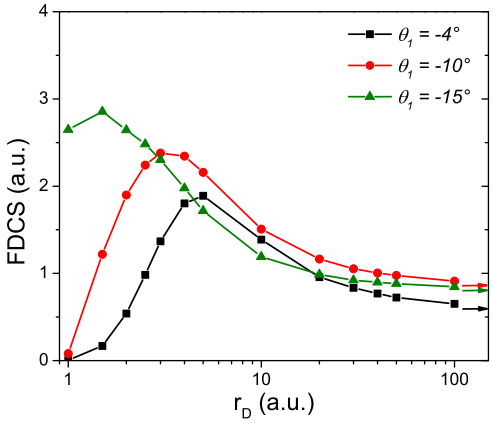

FIG. 10. Same as Fig. 4, but for $E_0 = 80$ eV and $E_2 = 10$ eV.

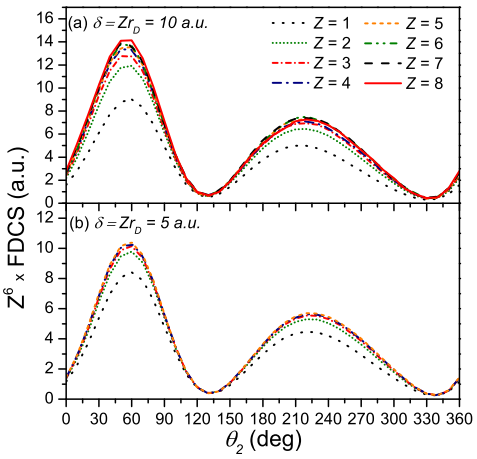

FIG. 11. Scaled fully differential cross section for electron impact ionization of several hydrogenic targets of charge Z as a function of the secondary electron emission angle into the scattering plane. The impact energy is $Z^2\times150$ eV, the secondary electron emission energy is $Z^2\times5$ eV and the projectile scattering angle is -4°.

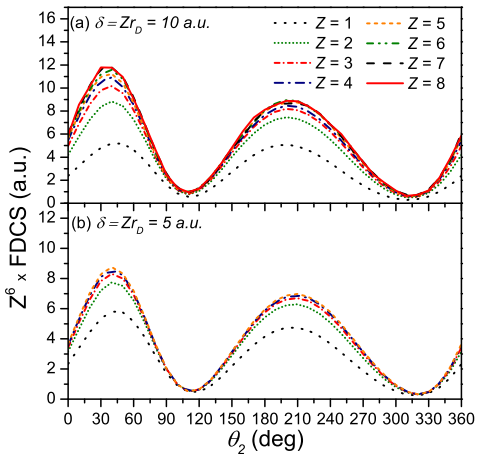

FIG. 12. Same as Fig. 11, but for an impact energy of $Z^2\times80$ eV.

account that at $r_D = 1$ a.u. the momentum transfer magnitudes are too small with respect to the emitted electron momentum.

Finally, we focus on the influence of the nuclear charge Z on the behavior of the FDCS for electron impact ionization of hydrogenic targets embedded in a Debye-Hückel plasma. Scaling laws involving the continuum of two-electron ions were first developed by Kornberg and Miraglia in the context of the photo-double ionization process[59], and later on generalized for fast electron impact ionization of unscreened hydrogenic and helium-like ions[60,61],

$$\frac{d^5\sigma}{dE_2 d\Omega_1 d\Omega_2}(E_0,Z) \rightarrow \frac{1}{Z^6}\frac{d^5\sigma}{d(E_2/Z^2)d\Omega_1 d\Omega_2}(E_0/Z^2,1).$$

In what follows, we analyze whether or not this scaling is still valid for hydrogenic targets embedded in Debye-Hückel plasmas. For these type of targets, Qi and co-workers[54] proposed the scaling transformations $\rho = Zr$, $\delta = Zr_D$ and $\varepsilon = E/Z^2$ to analyze the plasma screening effects on the properties of bound-bound transitions. In this sense, we employed the same transformations to our theoretical method in order to study the behavior of the FDCS.

In first place, we calculated the ionization FDCS of screened hydrogenic targets considering different values for the nuclear charge Z at an impact energy $E_0 = Z^2\times150$ eV, an emitted electron energy of $E_2 = Z^2\times5$ eV and a projectile scattering angle of -4°. The obtained results are presented for a fixed δ value of 10 a.u. and 5 a.u., in Fig. 11(a) and Fig. 11(b) respectively. Clear convergence is achieved as the nuclear charge Z increases. Similar results are obtained at the lower impact energy of $Z^2\times80$ eV hereby explored, and are shown in Fig. 12. In both cases, convergence seems to be attained faster for lower δ values. A point worth mentioning though, is that the scaling is meaningful only for $\delta > 0.83991$ or, in other words, when r_D is greater than the critical Debye radius for the Debye-Hückel potential[57].

IV. CONCLUSIONS

In this work, FDCS for electron impact ionizing collisions on atomic hydrogen embedded in weakly coupled plasmas were studied at impact energies of 80 eV and 150 eV. A Born-type distorted wave model which explicitly considers the screening effect among the three interacting particles in the final state was introduced and tested for different emission geometries.

Special emphasis was made in analyzing the sensitivity exhibited by the binary and recoil peaks, in both peaking position and width, to the degree of screening. As a result, for larger screenings binary peaks clearly reflect the Compton profile of the target. Recoil peaks, on the contrary, gain relevance as long as the screening decreases, provided that secondary collisions need a spatial window for momentum exchange to take place. Present results suggest that the magnitude of the binary peak, and the FDCS as a whole, seems to depend strongly on how similar or distinct are the projectile momentum transfer value and the emitted electron momentum under consideration.

A scaling law for the fully differential cross section in terms of the nuclear charge, first proposed by Kornberg and Miraglia in the photo-double ionization context, and later on proved

valid for electron impact ionization of H-like and He-like ions, has been shown to also hold in the present screened context.

Our work brings insight into the physical mechanisms that mediate electronic emission processes in Debye plasmas, and are therefore expected to be relevant for astrophysical and laboratory plasmas. In addition, the theoretical treatment hereby introduced can be naturally extended to other target systems, as long as it is restricted to the one-active electron approximation, and opens a challenging field for two (or more) active electron descriptions. It is our hope that the present findings will stimulate further experimental/theoretical work in the field.

ACKNOWLEDGMENTS

Work at IFISUR was supported by Grant No. PGI 24/F073, Secretaría General de Ciencia y Tecnología, Universidad Nacional del Sur, and Grant No. PIP 11220170100855CO of CONICET, Argentina.

DATA AVAILABILITY STATEMENT

The data that support the findings of this study are available from the corresponding author upon reasonable request.

REFERENCES

[1]R. C. Isler, "An overview of charge-exchange spectroscopy as a plasma diagnostic", Plasma Phys. Controlled Fusion **36**, 171 (1994).
[2]R. Hoekstra, H. Anderson, F. W. Bliek, M. von Hellerman, C. F. Maggi, R. E. Olson and H. P. Summers, "Charge exchange from D(n = 2) atoms to low- Z receiver ions", Plasma Phys. Controlled Fusion **40**, 1541 (1998).
[3]S. Otranto, R. E. Olson and P. Beiersdorfer, "X-ray emission cross sections following charge exchange by multiply charged ions of astrophysical interest", Phys. Rev. A **73**, 022723 (2006).
[4]S. Otranto, R. E. Olson and P. Beiersdorfer, "Cometary x-rays: line emission cross sections for multiply charged solar wind ion charge exchange", J. Phys. B: At. Mol. Opt. Phys. **40**, 1755 (2007).
[5]D. Bodewits, D. J. Christian, M. Torney, M. Dryer, C. M. Lisse, K. Dennerl, T. H. Zurbuchen, S. J. Wolk, A. G. G. M Tielens and R. Hoekstra, "Spectral analysis of the Chandra comet survey", Astron. Astrophys. **469**, 1183 (2007).
[6]U. Amaldi and G. Kraft, "Radiotherapy with beams of carbon ions", Rep. Prog. Phys. **68**, 1861 (2005).
[7]M. E. Galassi, C. Champion, P. F. Weck, R. D. Rivarola, O. Fojón and J. Hanssen, "Quantum-mechanical predictions of DNA and RNA ionization by energetic proton beams", Phys. Med. Biol. **57**, 2081 (2012).
[8]E. Alizadeh, T. M. Orlando, and L. Sanche, "Biomolecular Damage Induced by Ionizing Radiation: The Direct and Indirect Effects of Low-Energy Electrons on DNA", Annu. Rev. Phys. Chem. **66**, 379 (2015).
[9]A. V. Solov'yov, *Nanoscale Insights into Ion-Beam Cancer Therapy* (Springer, Berlin, 2017).
[10]N. Bachi, S. Otranto, G. S. Otero and R. E. Olson, "The role of multiple ionization of H_2O in heavy ion collisions", Phys. Med. Biol. **64**, 205020 (2019).
[11]H Ehrhardt, M Schulz, T Tekaat, and K Willmann, "Ionization of Helium: Angular Correlation of the Scattered and Ejected Electrons", Phys. Rev. Lett., **22**, 89 (1969).
[12]U. Amaldi, Jr., A. Egidi, R. Marcoreno, and G. Pizzella, "Use of a Two Channeltron Coincidence in a New Line of Research in Atomic Physics", Rev. Sci. Instrum. **40**, 1001 (1969).
[13]K. Jung, R. Muller-Fiedler, P. Schlemmer, H. Ehrhardt, and H. Klar, "Absolute triple differential cross sections of electron impact ionisation of helium at 600 eV collision energy", J. Phys. B: At. Mol. Opt. Phys. **18**, 2955 (1985).
[14]T Rösel, J Roder, L Frost, K Jung, and H Ehrhardt, "Measurement of absolute, near-threshold triple differential cross sections for electron impact ionization", J. Phys. B: At. Mol. Opt. Phys. **25**, 3859 (1992).
[15]X. Ren, S. Amami, O. Zatsarinny, T. Pflüger, M. Weyland, W. Y. Baek, H. Rabus, K. Bartschat, D. Madison, and A. Dorn, "Kinematically complete study of low-energy electron-impact ionization of neon: Internormalized cross sections in three-dimensional kinematics", Phys. Rev. A **91**, 032707 (2015).
[16]X. Ren, S. Amami, O. Zatsarinny, T. Pflüger, M. Weyland, A. Dorn, D. Madison, and K. Bartschat, "Kinematically complete study of low-energy electron-impact ionization of argon: Internormalized cross sections in three-dimensional kinematics", Phys. Rev. A **93**, 062704 (2016).
[17]M. A. Haynes and B. Lohmann, "Comparative study of argon $3p$ electron-impact ionization at low energies", Phys. Rev. A **64**, 044701 (2001).
[18]M. A. Stevenson and B. Lohmann, "Fully differential cross-section measurements for electron-impact ionization of argon over the complete in-plane angular range", Phys. Rev. A **77**, 032708(R) (2008).
[19]D. S. Milne-Brownlie, S. J. Cavanagh, B. Lohmann, C. Champion, P. A. Hervieux, and J. Hanssen, "Dynamics in electron-impact ionization of H_2O", Phys. Rev. A **69**, 032701 (2004).
[20]C. Kaiser, D. Spieker, J. Gao, M. Hussey, A. Murray, and D. H. Madison, "Coplanar symmetric and asymmetric electron impact ionization studies from the $1b_1$ state of H_2O at low to intermediate impact energies", J. Phys. B: At., Mol. Opt. Phys. **40**, 2563 (2007).
[21]X. Ren, S. Amami, K. Hossen, E. Ali, C. Ning, J. Colgan, D. Madison and A. Dorn, "Electron-impact ionization of H_2O at low projectile energy: Internormalized triple-differential cross sections in three-dimensional kinematics", Phys. Rev. A **95**, 022701 (2017).
[22]A. Lahmam-Bennani, E. M. Staicu Casagrande and A. Naja, "Experimental investigation of the triple differential cross section for electron impact ionization of N_2 and CO_2 molecules at intermediate impact energy and large ion recoil momentum", J. Phys. B: At. Mol. Opt. Phys. **42**, 235205 (2009).
[23]E. Ali, C. Granados, A. Sakaamini, M. Harvey, L. U. Ancarani, A. J. Murray, M. Dogan, C. Ning, J. Colgan, and D. Madison, "Triple differential cross sections for electron-impact ionization of methane at intermediate energy", J. Chem. Phys. **150**, 194302 (2019).
[24]X. Ren, T. Pflüger, S. Xu, J. Colgan, M. S. Pindzola, A. Senftleben, J. Ullrich, and A. Dorn, "Strong Molecular Alignment Dependence of H_2 Electron Impact Ionization Dynamics", Phys. Rev. Lett. **109**, 123202 (2012).
[25]D. H. Madison and O. Al-Hagan, "The Distorted-Wave Born Approach for Calculating Electron-Impact Ionization of Molecules", J. At. Mol. Phys. **2010**, 367180 (2010).
[26]M. Brauner, J. S. Briggs and H. Klar, "Triply-differential cross sections for ionisation of hydrogen atoms by electrons and positrons", J. Phys. B: At. Mol. Opt. Phys **22**, 2265 (1989).
[27]J. Berakdar and J. S. Briggs, "Three-body Coulomb continuum problem", Phys. Rev. Lett. **72**, 3799 (1994).
[28]C. Dal Cappello, Z. Rezkallah, S. Houamer, I. Charpentier, P. A. Hervieux, M. F. Ruiz-Lopez, R. Dey, and A. C. Roy, "Second-order Born approximation for the ionization of molecules by electron and positron impact", Phys. Rev. A **84**, 032711 (2011).
[29]O. Chuluunbaatar and B. Joulakian, "Three-centre continuum wavefunction: application to the (e, 2e) simple ionization of the $1\pi_g$, $1\pi_u$ and $3\sigma_u$ molecular orbitals of CO_2 by fast electron impact", J. Phys. B: At. Mol. Opt. Phys **43**, 155201 (2010).
[30]S. Jones and D. H. Madison, "Evidence of Initial-State Two-Center Effects for (e, 2e) Reactions", Phys. Rev. Lett. **81**, 2886 (1998).
[31]S. Jones and D. H. Madison, "Ionization of hydrogen atoms by fast electrons", Phys. Rev. A **62**, 042701 (2000).
[32]S. Otranto, "Initial-state correlation in the electron-impact ionization of argon", Phys. Rev. A **79**, 012705 (2009).
[33]E. Acebal and S. Otranto, "Continuum-distorted-wave eikonal-initial-state description of the electron-impact ionization of H_2O at low impact ener-

gies", Phys. Rev. A **98**, 012703 (2018).
[34]E. Acebal and S. Otranto, "Multicenter continuum-distorted-wave eikonal-initial-state description of the electron-impact ionization of aligned H_2 molecules", Phys. Rev. A **102**, 042808 (2020).
[35]D. S. F. Crothers and J. F. McCaan, "Ionisation of atoms by ion impact", J. Phys. B: At. Mol. Opt. Phys **16**, 3229 (1983).
[36]M. Baertschy, T. N. Rescigno, and C. W. McCurdy, "Accurate amplitudes for electron-impact ionization", Phys. Rev. A **64**, 022709 (2001).
[37]J. Colgan, M. Foster, M. S. Pindzola, I. Bray, A. T. Stelbovics, and D. V. Fursa, "Triple differential cross sections for the electron-impact ionization of helium at 102 eV incident energy", J. Phys. B: At. Mol. Opt. Phys. **42**, 145002 (2009).
[38]I. Bray, D. V. Fursa, A. S. Kadyrov, and A. T. Stelbovics, "Single ionization of helium by electron impact", Phys. Rev. A **81**, 062704 (2010).
[39]M. Dürr, C. Dimopoulou, A. Dorn, B. Najjari, I. Bray, D. V. Fursa, Z. Chen, D. H. Madison, K. Bartschat, and J. Ullrich, "Single ionization of helium by 102 eV electron impact: three-dimensional images for electron emission", J. Phys. B: At. Mol. Opt. Phys. **39**, 4097 (2006).
[40]S. D. Loch, C. J. Favreau, and M. S. Pindzola, "Electron-impact ionization of the Si atom", J. Phys. B: At. Mol. Opt. Phys. **52**, 055205 (2019).
[41]M. S. Pindzola and S. D. Loch, "Electron-impact ionization of the Kr atom", J. Phys. B: At. Mol. Opt. Phys. **52**, 245205 (2019).
[42]C. Granados-Castro and L. U. Ancarani, "Electron impact ionization of the outer valence orbital $1t_2$ of CH_4", Eur. Phys. J. D **71**, 65 (2017).
[43]R. K. Janev, S. Zhang and J. Wang, "Review of quantum collision dynamics in Debye plasmas", Matter and Rad. at Extr. **1**, 237 (2016).
[44]M. C. Zammit, D. V. Fursa and I. Bray, "Convergent-close-coupling calculations for excitation and ionization processes of electron-hydrogen collisions in Debye plasmas", Phys. Rev. A **82**, 052705 (2010).
[45]M. C. Zammit, D. V. Fursa, I. Bray and R. K. Janev, "Electron-helium scattering in Debye plasmas", Phys. Rev. A **84**, 052705 (2011).
[46]Y. Y. Qi, L. N. Ning, J. G. Wang and Y. Z. Qu, "Plasma effect on fast-electron-impact-ionization from $2p$ state of hydrogen-like ions", Phys. Plasmas **20**, 123301 (2013).
[47]J. Li, S. B. Zhang, B. J. Ye, J. G. Wang and R. K. Janev, "Low energy electron-impact ionization of hydrogen atom for coplanar equal-energy-sharing kinematics in Debye plasmas", Phys. Plasmas **23**, 123511 (2016).
[48]P. L. Bartlett and A. T. Stelbovics, "Threshold Behavior of e-H Ionizing Collisions", Phys. Rev. Lett. **93**, 233201 (2004).
[49]J. Berakdar, J. Röder, J. S. Briggs, and H Ehrhardt, J. Phys. B: At. Mol. Opt. Phys **29**, 6203 (1996).
[50]F. Salvat, J. M. Fernández-Varea, and W. Jr. Williamson, "Accurate numerical solution of the radial Schrödinger and Dirac wave equations", Comput. Phys. Commun. **90**, 151 (1995).
[51]C. R. Garibotti and J. E. Miraglia, "Ionization and electron capture to the continuum in the H^+-hydrogen-atom collision", Phys. Rev. A **21**, 572 (1980).
[52]T. Hahn, "CUBA—a library for multidimensional numerical integration", Comput. Phys. Commun. **168**, 78 (2005).
[53]A. W. Malcherek and J. S. Briggs, "The n-electron Coulomb continuum", J. Phys. B: At. Mol. Opt. Phys **30**, 4419 (1997).
[54]Y. Y. Qi, J. G. Wang and R. K. Janev, "Bound-bound transitions in hydrogenlike ions in Debye plasmas", Phys. Rev. A **78**, 062511 (2008).
[55]H. Ehrhardt, K. Jung, G. Knoth, and P. Schlemmer, "Differential Cross Sections of Direct Single Electron Impact Ionization", Z. Phys. D: At. Mol. Clusters **1**, 3 (1986).
[56]H. Ehrhardt and J. Röder, *Coincidence Studies of Electron and Photon Impact Ionization*, (Plenum, New York, 1997).
[57]F. J. Rogers, H. C. Graboske, Jr., and D. J. Harwood, "Bound Eigenstates of the Static Screened Coulomb Potential", Phys. Rev. A **1**, 1577 (1970).
[58]F. Biggs, L. B. Mendelsohn, and J. B. Mann, "Hartree-Fock Compton profiles for the elements", At. Data Nucl. Data Tables **16**, 201 (1975).
[59]M. A. Kornberg and J. E. Miraglia, "Scaling laws in double photoionization", Phys. Rev. A **49**, 5120 (1994).
[60]C. R. Stia, O. A. Fojón and R. D. Rivarola, "Ionization of hydrogenic targets by electron impact. Scaling laws", J. Phys. B: At. Mol. Opt. Phys **33**, 1211 (2000).
[61]A. L. Frapiccini, K. V. Rodríguez, G. Gasaneo and S. Otranto, "Electron Impact Single Ionization of the He-Isoelectronic Sequence", Braz. J. Phys. **37**, 1115 (2007).

Physics of Plasmas